IEEE Access
Multidisciplinary | Rapid Review | Open Access Journal

Received April 28, 2020, accepted May 7, 2020, date of publication May 12, 2020, date of current version May 29, 2020.

*Digital Object Identifier 10.1109/ACCESS.2020.2994219*

# Subsynchronous Oscillation Analysis of Grid-Connected Converter Based on MIMO Transfer Functions

**XIAOFANG WU, ZHENGCHUN DU, (Member, IEEE), XIAOTIAN YUAN, (Student Member, IEEE), GUIHONG WU, AND FENG ZENG**

School of Electrical Engineering, Xi'an Jiaotong University, Xi'an 710049, China

Corresponding author: Xiaofang Wu (xiaofangwu@stu.xjtu.edu.cn)

This work was supported by the National Key Research and Development Program of China under Grant 2017YFB0902000; in part by the Science and Technology Project of State Grid (SGXJ0000KXJS 1700841).

**ABSTRACT** Subsynchronous oscillations (SSOs) induced by the interaction between wind farms based on direct-drive permanent magnet synchronous generators (D-PMSGs) and weak grids have attracted extensive attention. To better understand this SSO phenomenon, this paper derives multi-input multi-output (MIMO) transfer functions between the references of the current controller and the current of a grid-connected converter in the *d-q* frame, where the dynamic of PLL is considered. The dynamic of PLL lead to positive feedback in the MIMO transfer function, which impairs the stability of the overall system and induces the SSO phenomenon. Using the classical root locus method, the influence of correlated control parameters and different operation conditions on the system stability is substantially analysed. It is found that heavy load, low short circuit ratio (SCR) will intensify the SSO instability of system. Nonlinear electromagnetic transient simulations of a D-PMSG-based weak-grid-connected wind-farm system using PSCAD/EMTDC software effectively verify the correctness of the model proposed in the SSO analysis.

**INDEX TERMS** Subsynchronous oscillations, D-PMSGs, MIMO transfer function, simulations.

## I. INTRODUCTION

The large-scale integration of wind energy into power grids worldwide is highly beneficial for relieving the energy crisis and environmental problems [1]–[3]. However, due to the uneven distribution of wind energy resources, long-distance AC lines are normally required to transfer wind energy to the load center, which may lead to a decreased SCR with a high penetration of wind energy [4]. The risk of subsynchronous oscillations (SSOs) due to SCR changes therefore increases, which has impaired the stability of the power system in recent days [5]. Therefore, how to analyse and suppress the SSOs introduced by the grid integration of wind energy conversion systems (WECSs) with weak AC systems has been a great challenge for further large-scale wind application.

Many studies have focused on analysing the mechanism of SSOs and suppressing SSOs. Generally, there are three methods for studying the SSO phenomenon that occurs due to the large-scale integration of WECSs into weak AC systems, namely, electromagnetic transient (EMT) simulation, mode analysis, and impedance analysis [2]–[8]. The EMT simulation method can visually observe the dynamic characteristics of a wind farm under given grid scenarios. However, this method is usually time-consuming. To overcome the shortcoming, the latter two methods are proposed, which can directly identify the potential instability modes of WECSs.

In the mode analysis based method, the oscillation modes of the system can be easily obtained through eigenvalue analysis, and the main influencing factors can be clearly identified by comparing each participation factor of the system matrix. This method is widely used in analysing SSOs induced by different types of wind generators, such as wind farms with doubly fed induction generators [2]–[5] or permanent magnet synchronous generators (PMSGs) [6]–[8]. One study [4] studied the influence of wind farms' spatial distribution and the compensation level of parallel transmission lines on SSOs

The associate editor coordinating the review of this manuscript and approving it for publication was Heng Wang.

using mode analysis. Another study [5] established a case study with several transmission lines (many of them series compensated), various conventional and wind power plants, and a distributed load. Then the subsynchronous interaction among various wind farms and transmission lines is studied using eigenvalues and time-domain simulations. Although the mode analysis based method great insight into SSO phenomenon, its applicability for SSO analysis is usually limited as it is hard to analyse the factors that lead to system instability and to disclose the mechanism of the SSO phenomenon.

Impedance analysis is also widely used in studying the SSO phenomenon of WECSs. In this method, a wind generator can be simplified as an input-impedance by the derivation of the terminal current change with respect to the voltage change through a small-signal-analysis method. Then the SSO stability can be easily analysed by classical control theory methods such as the root locus method and the Nyquist criterion method [9]–[12]. One study [9] proposed an SSR stability analysis method based on an impedance network model. The impedance models of each wind farm and transmission line are established, and then interconnected according to the system topology to form the whole impedance network model, which is further aggregated into the lumped impedance. The SSO stability criterion is developed by analysing the impedance-frequency features of the lumped impedance. Some studies [13], [14] gave the full impedance model of the grid-connected inverter considering the current feedback control and phase lock loop (PLL) dynamic in the frame. The model shows that the PLL shapes a *q*-*q* channel output impedance of the grid-connected inverter as a negative incremental resistor within its bandwidth. Similar to the model analysis based method, the impedance analysis based method can assess the stability of the system but lacks the ability to explain the mechanism of the SSOs.

To reveal the mechanism of the SSOs clearly, some studies derived the response characteristics of the converter to the subsynchronous signals, which can explain the mechanism of the SSOs in D-PMSG to some degree [16]–[20]. Deriving the analytical expressions for output signals when the input signals of the PLL and d-q decoupling control system are superimposed with a subsynchronous frequency component explained why the currents have multiple frequency components when SSOs occur [16], [17]. Taking into account the control system of the converter and the AC system, the single-input and single-output (SISO) transfer function of the D-PMSG grid-connected system were derived in [18], which provides the reasons for the sub- and super-synchronous frequency components from the stability of the control system. However, it is difficult for the SISO transfer function to accurately reflect the subsynchronous frequency response characteristics of the converter controller as its d- and q-axis are coupled. One study [19] completely explained how the coupling characteristics affect the converter response. To this end, another study [20] derived the two-input and two-output (TITO) transfer functions of a D-PMSG grid-connected system, which was verified as more accurate than the SISO transfer function. Regrettably, this study focused on the amplitude-frequency characteristics of the converter's output voltage under the disturbance current and may not sufficiently reflect the SSO stability of the system. Study [21], [22] derived a complete SISO model from the MIMO model, for the stability analysis of grid-connected VSC in a weak-grid condition. And then use the standard SISO Nyquist stability criterion for the stability analysis of grid-connected VSCs. As a mature method, MIMO transfer function has been widely used in the analysis and control of multi - input multi-output system, which is comprehensive and intuitive.

This paper analyses the mechanism of the SSO phenomenon by building a model between the references of the current controller and the current of the grid-connected converter in the d-q frame through multi-inputs multi-outputs (MIMO) transfer functions. By deriving the MIMO transfer function, the mathematical expression of input and output of D-PMSG is established, which helps us clearly understand the mechanism of subsynchronous. In addition, by comparing the MIMO transfer function with and without the PLL dynamic, the influence of PLL dynamics on system stability can be clearly explained, which can't be easily indicated by the mode analysis based method The main contributions of this paper are presented as follows:

Firstly, based on the open-loop transfer functions including the PLL and controllers, the MIMO transfer functions considering both the d-axis channel and q-axis channel are derived, which fully considers the d- and q-axis coupling characteristics of the control system.

Secondly, the root locus of the transfer function is calculated subsequently to analyse the influence of different parameters and operation conditions on the SSOs.

Finally, the detailed electromagnetic transient simulation model of the D-PMSG grid-connected equivalent system is built using the PSCAD/EMTDC simulation tool, and the transient simulation is carried out to verify the root locus analysis results.

## II. MIMO TRANSFER FUNCTIONS OF THE D-PMSG GRID-CONNECTED SYSTEM

### A. MODEL OF THE D-PMSG GRID-CONNECTED SYSTEM

A D-PMSG is composed of a wind turbine, a PMSG, a full power converter, and a filter. It is widely acknowledged that the subsynchronous interaction between D-PMSG and weak ac grid is mainly induced by the control features of GSC [7]. Hence, a simplified equivalent modal of the D-PMSG-based grid-connected system is establish in this paper, i.e. an ideal DC voltage source is connected to an infinite AC voltage source through a single inverter and a grid inductance. The block diagram of the studied system is shown in Fig.1. The control system consists of the PLL, the *d*-*q* decoupling current controller, and the PWM [11].

The current controller achieves its control goals by controlling the ratio of the *d*- and *q*-axis measurement currents of the

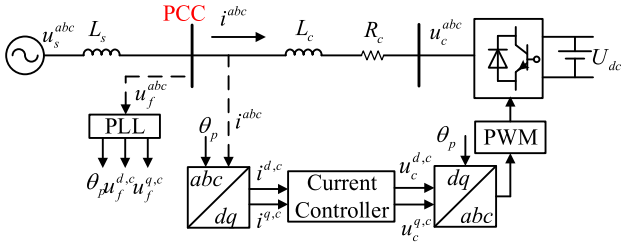


**FIGURE 1.** The D-PMSG grid-connected system.

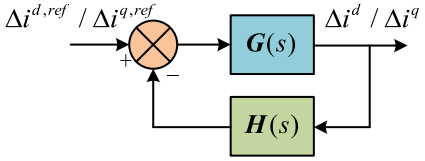


**FIGURE 2.** Diagram of MIMO transfer functions.

point of common coupling (PCC) voltages, $i^{d,c}/i^{q,c}$. When a disturbance occurs in the system, disturbance components $i_{dss1}/i_{dss2}$ will be superimposed on $i^{d,c}/i^{q,c}$. The $i_{dss1}/i_{dss2}$ enter the system through the current controller and flow in all parts of the controllers and the electrical system, thus affecting other variables of the system. As an input of the current controller, the $i_{dss1}/i_{dss2}$ can be regarded as the small signal variable of the current reference $i^{d,ref}/i^{q,ref}$. Therefore, the above system can be equivalent to a MIMO system from $\Delta i^{d,ref}/\Delta i^{q,ref}$ to $\Delta i^{d}/\Delta i^{q}$, as shown in Fig. 2. This paper studies the SSO phenomenon by deriving the MIMO transfer functions shown in Fig. 2, where $\boldsymbol{G}(s)$ is the open-loop transfer function and $\boldsymbol{H}(s)$ is the negative feedback function. Both functions are second-order square matrixes. The closed-loop transfer function is defined as follows:

$$\boldsymbol{G}_T(s) = \frac{\boldsymbol{G}(s)}{\boldsymbol{I} + \boldsymbol{G}(s)\boldsymbol{H}(s)} = \begin{bmatrix} G_{dd} & G_{dq} \\ G_{qd} & G_{qq} \end{bmatrix} \tag{1}$$

The stability of the studied system can be determined by the poles of the MIMO transfer functions.

To study the influence of the PLL on the system stability, this paper derives the MIMO transfer functions considering the dynamic of the PLL. The MIMO transfer functions that does not consider the dynamic of the PLL will also be given for comparison; it can be derived based on the former MIMO transfer functions and regarded as a simplified form under special conditions.

### *B. MIMO TRANSFER FUNCTIONS CONSIDERING THE PLL*

As an indispensable part of the D-PMSG, the dynamic of the PLL has an essential effect on the studied system; therefore, it's necessary to take the PLL into account when forming the MIMO transfer functions. The MIMO transfer functions that consider the dynamic of the PLL are established on the foundation of the small signal model of the control system and the AC transmission system.

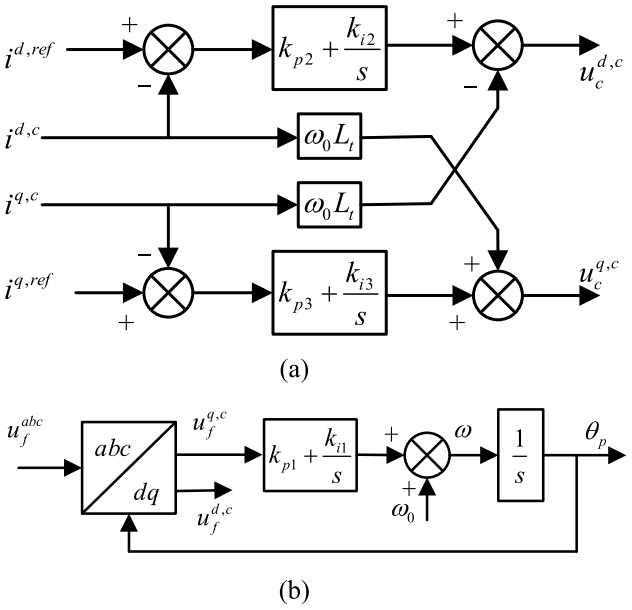


**FIGURE 3.** Control system: (a) control block diagram of current controller, and (b) control block diagram of PLL.

#### 1) MODEL OF THE CURRENT CONTROLLER

Fig. 3a shows the diagram of the current controller. The dynamic process of the outer voltage loop of the controller is ignored in this paper, due to its faster response compared with that of the inner current control loop [13], [17]. To highlight the influence of the PLL, this study assumes that $L_t = L_c + L_s$ [19], where $L_c$ is the terminal inductance of the D-PMSG and $L_s$ is the equivalent connection inductance between the PCC and the infinite AC voltage source. The mathematical equation of the current controller can be expressed as follows:

$$\begin{cases} \Delta u_c^{d,c} = (k_{p2} + \dfrac{k_{i2}}{s})(\Delta i^{d,ref} - \Delta i^{d,c}) - \omega_0 L_t \Delta i^{q,c} \\ \Delta u_c^{q,c} = (k_{p3} + \dfrac{k_{i3}}{s})(\Delta i^{q,ref} - \Delta i^{q,c}) + \omega_0 L_t \Delta i^{d,c} \end{cases} \tag{2}$$

where $k_{p2}$ and $k_{p3}$ are the proportional gains of the current controller, $k_{i2}$ and $k_{i3}$ are the integral gains of the current controller, $\omega_0$ is the electrical angular frequency of the system, and $s$ is the differential operator.

#### 2) MODEL OF THE PLL

The typical structure of the PLL is shown in Fig. 3b. There will be two different rotating reference $d$-$q$ frames: one is the system $d$-$q$ frame, and another is the controller $d^c$-$q^c$ frame [14], both of which are shown in Fig. 4. The $d$-$q$ frame is defined by the phase information of grid voltage $u_{abc}$, and the controller $d^c$-$q^c$ frame is defined by the output of the PLL, which estimates the frequency and angle of the grid voltage to track the position of the system $d$-$q$ frame. Under a stable condition, the output of the PLL agrees with the actual information of the grid voltage, and the phases of the system $d$-$q$ frame and the controller $d^c$-$q^c$ frame are aligned.

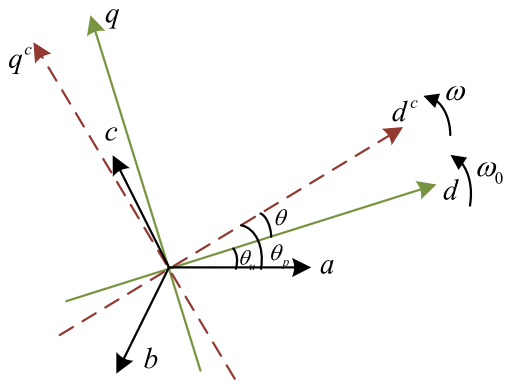


**FIGURE 4.** Two different *d-q* frames: the *d-q* frame and dc-qc frame.

When a disturbance is added to the grid voltage, the position of the system $d$-$q$ frame is changed. And, the controller $d^c$-$q^c$ frame will no longer agree with the system $d$-$q$ frame because of the dynamic of the PLL. There will be a phase difference between the two $d$-$q$ frames, named $\theta$ as shown in Fig. 4, which can be expressed as follows:

$$\Delta\theta = (k_{p1} + \frac{k_{i1}}{s})\frac{1}{s}\Delta u_f^{q,c} \tag{3}$$

where $k_{p1}$ and $k_{i1}$ are the proportional gains and the integral gains of the PLL, respectively.

The voltage and current vectors in the system $d$-$q$ frame are rotated to the vectors in the controller $d^c$-$q^c$ frame by matrix $\boldsymbol{T}_\theta$. The duty-cycle commands generated by the controller are then rotated to the system $d$-$q$ frame by the inverse of matrix $\boldsymbol{T}_\theta$ to control the power semiconductors [14].

$$\boldsymbol{T}_\theta = \begin{bmatrix} \cos\theta & \sin\theta \\ -\sin\theta & \cos\theta \end{bmatrix} \tag{4}$$

$$\boldsymbol{u}_f^c = \boldsymbol{T}_\theta \boldsymbol{u}_f, \quad \boldsymbol{i}^c = \boldsymbol{T}_\theta \boldsymbol{i}, \ \boldsymbol{u}_c^c = \boldsymbol{T}_\theta \boldsymbol{u}_c \tag{5}$$

where $\boldsymbol{u}_f$, $\boldsymbol{i}$, and $\boldsymbol{u}_c$ are the voltage of PCC, and current of PCC and the terminal voltage of converter in the system $d$-$q$ frame, respectively, and $\boldsymbol{u}_f^c$, $\boldsymbol{i}^c$, and $\boldsymbol{u}_c^c$ are the corresponding vectors in the controller $d^c$-$q^c$ frame. Note that if the PLL is ideal, $\theta$ will be zero, and $\boldsymbol{T}_\theta$ will be a unit matrix.

In a stable condition, the initial value of the voltage and current vectors is as follows:

$$\theta = 0, u_{f0}^d = 1, u_{f0}^q = 0, \ i_0^d = i^{d,ref}, \ i_0^q = i^{q,ref} = 0 \tag{6}$$

The linearization of (5) is as follows:

$$\begin{cases} \Delta u_f^d = \Delta u_f^{d,c} \\ \Delta u_f^q = \Delta u_f^{q,c} + u_{f0}^d \Delta\theta \end{cases} \tag{7}$$

$$\begin{cases} \Delta u_c^d = \Delta u_c^{d,c} \\ \Delta u_c^q = \Delta u_c^{q,c} + u_{c0}^d \Delta\theta \end{cases} \tag{8}$$

$$\begin{cases} \Delta i^d = \Delta i^{d,c} \\ \Delta i^q = \Delta i^{q,c} + i_0^d \Delta\theta \end{cases} \tag{9}$$

Substituting (7) into (3), the transfer function of the PLL can be obtained:

$$\begin{aligned} \Delta\theta &= G_{PLL}(s)\Delta u_f^q \\ G_{PLL}(s) &= \frac{k_{p1}s + k_{i1}}{s^2 + k_{p1}s + k_{i1}} \end{aligned} \tag{10}$$

### 3) MODEL OF THE AC TRANSMISSION SYSTEM

In the system $d-q$ frame, the voltage balance equation of the AC transmission system can be expressed as follows:

$$\begin{cases} \Delta u_c^d = sL_t\Delta i^d - \omega_0 L_t \Delta i^q \\ \Delta u_c^q = \omega_0 L_t \Delta i^d + sL_t \Delta i^q \end{cases} \tag{11}$$

$$\begin{cases} \Delta u_f^d = sL_g\Delta i^d - \omega_0 L_g \Delta i^q \\ \Delta u_f^q = \omega_0 L_g \Delta i^d + sL_g \Delta i^q \end{cases} \tag{12}$$

Substituting (12) into (10), $\theta$ can be represented in terms of $\boldsymbol{i}$:

$$\Delta\theta = \omega_0 G_{PLL}(s)L_t\Delta i_d + sG_{PLL}(s)L_g\Delta i_q \tag{13}$$

### 4) MIMO TRANSFER FUNCTIONS CONSIDERING THE PLL

Based on the models of each part above, the MIMO transfer functions including the dynamic of the PLL can be derived. Combining (2), (7)-(9), (11), and (13),

$$\begin{aligned} \boldsymbol{G}(s) &= \begin{bmatrix} G_{11}(s) & 0 \\ 0 & G_{22}(s) \end{bmatrix} \\ \boldsymbol{H}(s) &= \begin{bmatrix} H_{11}(s) & H_{12}(s) \\ H_{21}(s) & H_{22}(s) \end{bmatrix} \end{aligned} \tag{14}$$

The individual subtransfer functions are given by the following:

$$\begin{cases} G_{11}(s) = (sk_{p2} + k_{i2})/s^2L_t \\ G_{22}(s) = (sk_{p3} + k_{i3})/s^2L_t \\ H_{11}(s) = 1 - sk_1\omega_0 G_{PLL}(s)/(sk_{p2} + k_{i2}) \\ H_{12}(s) = -k_2\omega_0 G_{PLL}(s) - sk_3\omega_0 G_{PLL}(s)/(sk_{p3} + k_{i3}) \\ H_{21}(s) = s^2k_1 G_{PLL}(s)/(sk_{p2} + k_{i2}) \\ H_{22}(s) = 1 - sk_2 G_{PLL}(s) - s^2k_3 G_{PLL}(s)/(sk_{p3} + k_{i3}) \end{cases} \tag{15}$$

where $k_1 = \omega_0 L_t i^{d,ref}$, $k_2 = L_g i^{d,ref}$, and $k_3 = v_{d0}L_g$.

It can be seen from (15) that the forward transfer function $\boldsymbol{G}(s)$ is related to the current controller and the equivalent inductance. The feedback transfer function $\boldsymbol{H}(s)$ consists of a unit negative feedback and a positive feedback that is mainly related to the PLL.

Substituting (14) into (1) gives the closed-loop transfer function considering the dynamic of the PLL, as follows:

$$\boldsymbol{G}_{\mathrm{T}}(s) = \frac{\boldsymbol{G}(s)}{\boldsymbol{I} + \boldsymbol{G}(s)\boldsymbol{H}(s)} = \begin{bmatrix} G_{dd} & G_{dq} \\ G_{qd} & G_{qq} \end{bmatrix} \tag{16}$$

The individual subtransfer functions are given by the following:

$$\begin{cases} G_{dd} = \dfrac{G_{11}(1+G_{22}H_{22})}{(1+G_{11}H_{11})(1+G_{22}H_{22})-G_{11}G_{22}H_{12}H_{21}} \\ G_{dq} = \dfrac{-G_{11}^2H_{12}}{(1+G_{11}H_{11})(1+G_{22}H_{22})-G_{11}G_{22}H_{12}H_{21}} \\ G_{qd} = \dfrac{-G_{22}^2H_{21}}{(1+G_{11}H_{11})(1+G_{22}H_{22})-G_{11}G_{22}H_{12}H_{21}} \\ G_{qq} = \dfrac{G_{22}(1+G_{11}H_{11})}{(1+G_{11}H_{11})(1+G_{22}H_{22})-G_{11}G_{22}H_{12}H_{21}} \end{cases} \tag{17}$$

It can be seen from (16) and (17) that the MIMO transfer functions are coupled and unsymmetrical when the dynamic of the PLL is considered.

### C. MIMO TRANSFER FUNCTIONS WITHOUT CONSIDERING THE PLL

When the PLL can ideally track the phase of $u_{abc}$, the controller $d^c$-$q^c$ frame will be always aligned with the system $d$-$q$ frame. The output of the PLL, that is $\theta$, is zero, and the corresponding transfer function of the PLL is as follows:

$$G_{PLL}(s) = \frac{\Delta\theta}{\Delta u_f^{q,c}} = 0 \tag{18}$$

Substituting (18) into (15), the open-loop transfer function of the control system when the PLL is ignored is as follows:

$$\begin{cases} G'_{11}(s) = G'_{22}(s) = (sk_{p2}+k_{i2})/s^2L_t \\ H'_{11}(s) = H'_{22}(s) = -1 \\ H'_{12}(s) = H'_{21}(s) = 0 \end{cases} \tag{19}$$

Comparing (19) to (15), the forward transfer function of the control system is the same whether the PLL is considered or not. The idealisation of the PLL allows us to ignore the positive feedback in the feedback transfer function $\boldsymbol{H}(s)$.

Substituting (19) into (1), the MIMO transfer function without considering the dynamic of the PLL, $\boldsymbol{G'}_{\mathrm{T}}(s)$, can be expressed as follows:

$$\boldsymbol{G'}_{\mathrm{T}}(s) = \frac{\boldsymbol{G'}(s)\boldsymbol{H'}(s)}{\boldsymbol{I}-\boldsymbol{G'}(s)\boldsymbol{H'}(s)} = \begin{bmatrix} G'_{dd} & 0 \\ 0 & G'_{qq} \end{bmatrix} \tag{20}$$

$$G'_{dd} = G'_{qq} = \frac{sk_{p2}+k_{i2}}{s^2L_t+sk_{p2}+k_{i2}} \tag{21}$$

When the dynamic of the PLL is neglected, the MIMO control system from $\Delta i^{d,ref}/\Delta i^{q,ref}$ to $\Delta i^d/\Delta i^q$, is a closed-loop system with negative feedback, and the closed-loop transfer function is decoupled and symmetrical.

## III. ANALYSIS OF SUBSYNCHRONOUS OSCILLATIONS

In this section, the mechanism of the SSO phenomenon in the D-PMSG grid-connected system is analysed based on the MIMO transfer functions. The root locus of the transfer function is calculated to analyse the influence of related parameters on the SSO stability.

### A. SSOs MECHANISM OF THE D-PMSG GRID-CONNECTED SYSTEM

Without considering the dynamic of the PLL, the controller $d^c$-$q^c$ frame is aligned with the system $d$-$q$ frame. Assuming that the inverter is directly connected to the ideal power supply without impedance, there is a basic closed-loop negative feedback structure between the reference current and the grid current, which is shown in (20). The two poles of the closed-loop transfer function $\boldsymbol{G'}_{\mathrm{T}}(s)$ are as follows:

$$s_{1,2} = \frac{-k_{p2} \pm \sqrt{k_{p2}^2 - 4L_tk_{i2}}}{2L_t} \tag{22}$$

Usually, $k_{p2}$ is much smaller than $k_{i2}$. The closed-loop transfer function has a pair of complex poles when the dynamic characteristics of the PLL are ignored, whose real part is negative. The system will be considered stable without considering the dynamic characteristics of the PLL. However, the conclusion may be wrong when the dynamic of the PLL is taken into consideratiom.

Equations (14)-(17) indicate that the dynamic of the PLL introduces positive feedback to the closed-loop transfer function, which creates the possibility of instability in the system. It can be seen from (15) that the positive feedback is strongly correlated with the system operating conditions, the PLL, and the current controller. The system becomes unstable when the unit negative feedback cannot counteract the effect of the positive feedback under certain parameter combinations or specific operating conditions.

The control theory indicates that a system has output stability if and only if all the poles of its transfer functions located in the left part of the $s$ plane [23]. It can be further confirmed that the subtransfer functions in (17) have the same denominator, which is to say that they have the same stability domain. In this paper, the root locus method is used to analyse the influence of parameters and operation conditions on the stability of the D-PMSG grid-connected system.

### B. ANALYSIS OF MIMO CLOSED-LOOP TRANSFER FUNCTIONS

This paper takes the typical single-machine infinite bus D-PMSG grid-connection system as the system being studied. The basic parameters are shown in Table 1.

**TABLE 1. The parameters of the system.**

| Parameter | Value | Parameter | Value |
|---|---|---|---|
| $S_B$ (MVA) | 2.0000 | $V_B$ (kV) | 0.8200 |
| $\omega_0$ (rad/s) | 314.15 | $i^{d,ref}$ (p.u.) | 1.0000 |
| $L_c$(mH) | 0.1500 | $L_s$ (mH) | 0.6500 |
| $k_{p1}$ | 0.0850 | $k_{i1}$ | 32.000 |
| $k_{p2}$ | 0.2000 | $k_{i2}$ | 355.00 |
| $k_{p3}$ | 0.2000 | $k_{i3}$ | 355.00 |

According to those parameters, the poles of $\boldsymbol{G}'_{\mathrm{T}}(s)$ are easily calculated as follows:

$$s_{1,2} = -153.84 \pm 772.83i \tag{23}$$

These values reflect a positively damped super-synchronous oscillation mode with a frequency of about 122.99Hz. The system is stable without considering the dynamic of the PLL. However, the conclusion may be wrong when the dynamic of the PLL is taken into consideration.

The order of the MIMO closed-loop transfer function that considers the dynamic of the PLL (i.e., $\boldsymbol{G}_{\mathrm{T}}(s)$) is six, and it has three pairs of complex poles ($s_{1,2}$, $s_{3,4}$ , $s_{5,6}$), while there is just a pair of positively damped complex poles in $\boldsymbol{G}'_{\mathrm{T}}(s)$. The poles of the MIMO transfer functions at the initial parameters are shown in Table 2. Table 2 indicates that there is a negatively damped SSO mode (corresponding to $s_{5,6}$) with a frequency of about 23Hz, which is ignored in the transfer function that doesn't consider the dynamic of the PLL. It can be concluded that the dynamic of the PLL may cause SSO instability.

**TABLE 2. Poles of the MIMO transfer functions.**

| Number | Pole |
|---|---|
| $s_{1,2}$ | −128.511 ± 622.870i |
| $s_{3,4}$ | −129.870 ± 666.463i |
| $s_{5,6}$ | 4.63737 ± 145.374i |

In this section, different system parameters and operation conditions are considered in drawing the root locus of the obtained MIMO transfer functions. The imaginary parts of the poles are replaced by oscillation frequencies, which are equal to the imaginary parts over $2\pi$.

### 1) THE IMPACT OF THE OPERATION CONDITION

Change the current reference $i^{d,ref}$ from 0.5 p.u. to 1.1 p.u. and a pair of complex poles ($s_{5,6}$) will change significantly; its root locus is shown in Fig. 5. Note that the horizontal axis refers to the real part of the poles of the MIMO transfer functions, while the vertical axis is the oscillation frequency.

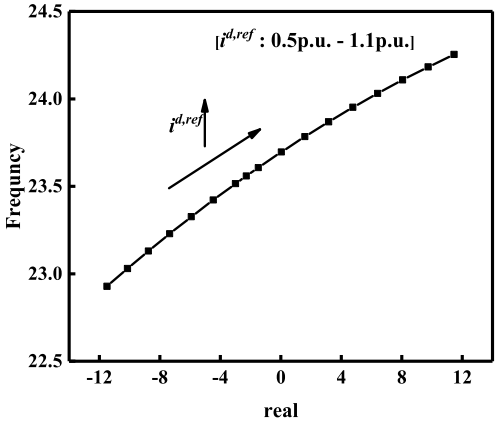


**FIGURE 5. Root locus ($s_5$) of studied system as $i^{d,ref}$ changes.**

Clearly, as $i^{d,ref}$ increases, which means a heavier load, the real part of $s_{5,6}$ increases gradually, and changes from negative to positive. In other words, a heavy load may induce SSO instability in a grid-connected D-PMSG. Moreover, the rise of $i^{d,ref}$ leads to a higher oscillation frequency.

### 2) THE IMPACT OF THE EQUIVALENT INDUCTANCE

The connection inductance between the PCC and the ideal power supply (i.e., Ls) as a reflection of the SCR has an important impact on SSOs. Fig. 6 demonstrates the effect of the SCR on the poles corresponding to the SSO mode, i.e., s5,6. As illustrated in Fig. 6, the increase in Ls drives the concerned poles across the imaginary axis to the right region. That is to say, a low SCR can weaken the stability of the SSO mode, and its frequency decreases slightly.

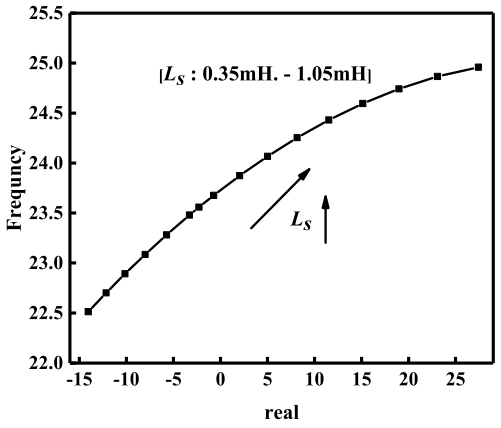


**FIGURE 6. Root locus ($s_5$) of studied system as $L_S$ changes.**

### 3) THE IMPACT OF THE PLL

As already discussed, among the controllers of the D-PMSG, the PLL shows a significant impact on the SSO. Fig. 7 shows the variation of $s_{5,6}$ while the proportionality gain of the PLL (i.e., $k_{p1}$) changes from 0.03 to 0.1. The damping and frequency of the SSO have a positive correlation with $k_{p1}$.

Fig. 8 displays the impact of the integral gain of the PLL (i.e., $k_{i1}$) on the poles corresponding to the SSO mode

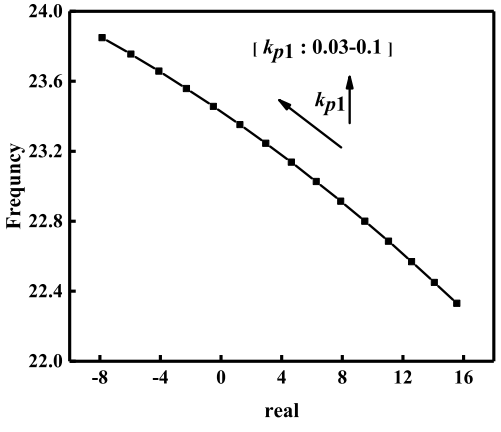


**FIGURE 7. Root locus ($s_5$) of studied system as $k_{p1}$ changes.**

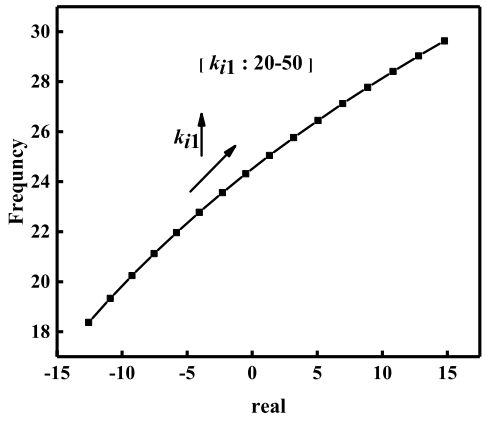


**FIGURE 8.** Root locus ($s_5$) of studied system as $k_{i1}$ changes.

($s_{5,6}$). As opposed to $k_{p1}$, with $k_{i1}$ adding from 20 to 50, the parameters of the PLL greatly impact the SSO stability of the D-PMSG grid-connected system. An increase in the proportionality gain or a decrease in the integral gain of the PLL can enhance the stability of the SSO mode.

#### 4) THE IMPACT OF THE CURRENT CONTROLLER

Increasing the proportionality gain of the current controller (i.e., $k_{p2}$) from 0.12 to 0.27 will change two pairs of complex poles ($s_{1,2}$, $s_{3,4}$); the root locus is shown in Fig. 9. When the integral gain of the current controller (i.e., $k_{i2}$) ranges from 200 to 390, the root locus is as shown in Fig. 10. As Fig. 9 shows, the change of $k_{p2}$ mainly influences the super-synchronisation oscillation of the system; however, the small change in $s_{1,2}$ and $s_{3,4}$ doesn't destabilise the system. Fig. 10 reveals that the reduction of $k_{i2}$ increases the real part of the pole corresponding to the SSO mode or even makes it positive. The decrease in $k_{i2}$ drives the SSO mode, $s_{5,6}$, towards the unstable region.

## IV. SIMULATION VERIFICATION

To verify the theoretical analysis above, the detailed electromagnetic transient simulation model of the system studied in Fig. 1 is built with the PSCAD/EMTDC software.

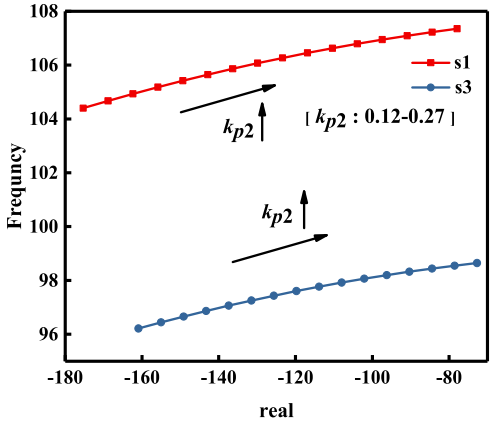


**FIGURE 9.** Root locus ($s_1$, $s_3$) of studied system as $k_{p2}$ changes.

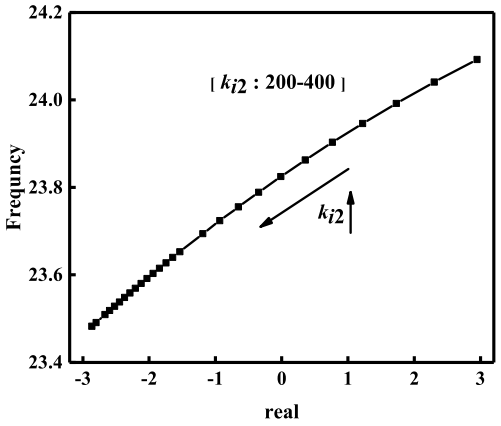


**FIGURE 10.** Root locus ($s_5$) of studied system as $k_{i2}$ changes.

The basic parameters of the D-PMSG system are shown in Table 1. According to the analysis in Section 3, four cases will be carried out. For each case, the initial connection inductance between the PCC point and ideal power is set as 0.2 mH to ensure the simulation starts from the stable state. Then the inductance is increased to motivate the SSO.

### A. THE IMPACT OF THE EQUIVALENT INDUCTANCE

In this case, the equivalent inductance is added to 0.3mH at 1s, and to 0.65mH at 3s, which makes the SCR of the AC system decline gradually.

The simulation lasts for 4.5s. The curves of the phase-A current and active power of the PCC are displayed in Fig. 11 (a) and (b). A stage change in the equivalent inductance induces the observed signals to oscillate immediately. When the equivalent inductance is at 0.5mH, the oscillation tends to be convergent, and transits to another steady state after about 0.6s. Relatively, the oscillation tends to be divergent at 0.65mH. As the equivalent inductance increases, the oscillation diverges, which matches the analysis of the root locus, that the weak AC grid makes the system SSOs unstable.

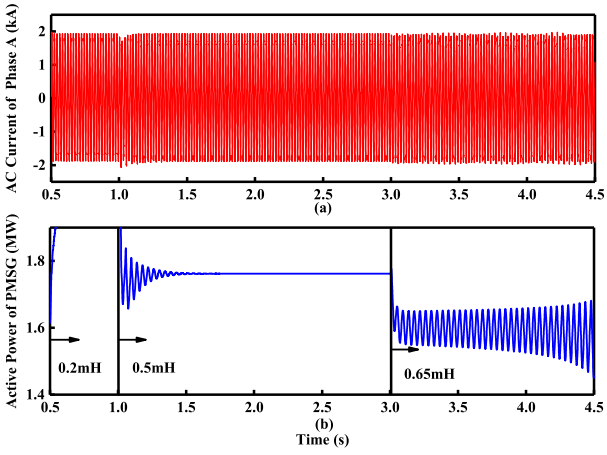


**FIGURE 11.** AC current and active power of the D-PMSG grid-connected system: (a) AC current, and (b) active power.

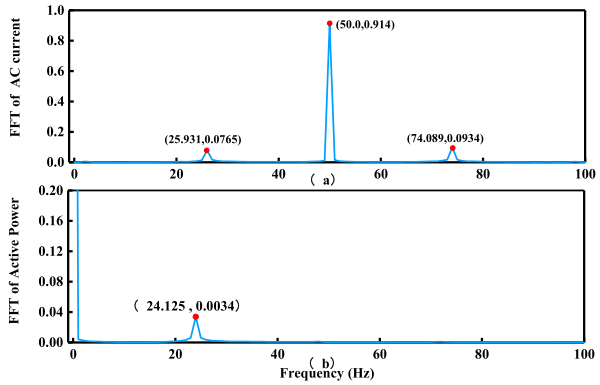


**FIGURE 12.** DFT of waves of AC current and active power: (a) AC current, and (b) active power.

A spectrum analysis based on a discrete Fourier transformation (DFT) is carried out for the output current and active power waveforms, and the results are shown in Fig. 12 (a) and (b). Fig. 12 indicates that the current curve has a subsynchronous component of 26Hz and a super-synchronous component of 74Hz, while the active power has a subharmonic component with the complementary frequency (50Hz –26Hz = 24Hz), which is in accordance with the analysis of the transfer function.

### B. THE IMPACT OF THE OPERATION CONDITION

Keeping the other parameters unchanged and reducing $i^{d,ref}$ gives the oscillation waveforms of the active power of the system as shown in Fig. 13. The yellow line, red line, and blue line are the active powers of the D-PMSG system when $i^{d,ref}$ is 1.0, 0.9, and 0.8p.u., respectively. The increase in the reference current reduces the stability of the system.The simulation results above agree with the root locus analysis of the MIMO transfer function poles.

### C. THE IMPACT OF THE PROPORTIONAL GAIN OF THE PLL

To study the oscillation characteristics influenced by the proportional gain of the PLL, $k_{p1}$ was set to 0.075, 0.09, 0.085, 0.09, and 0.095, giving the oscillation waveforms of the active power of the system as illustrated in Fig. 14. Fig. 14 shows that a decrease in $k_{p1}$ distinctly weakens the stability so that the waveform of the active power diverges more quickly. This result matches the root locus analysis in Section 3.2.3 well.

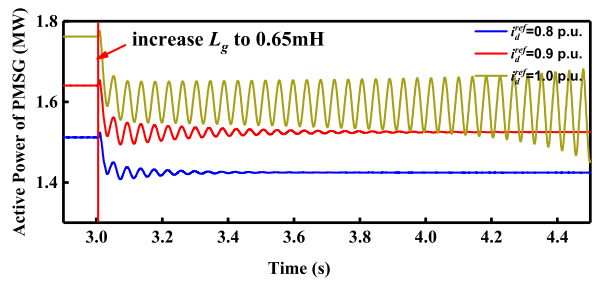


**FIGURE 13.** Active power of the D-PMSG grid-connected system as $i^{d,ref}$ changes.

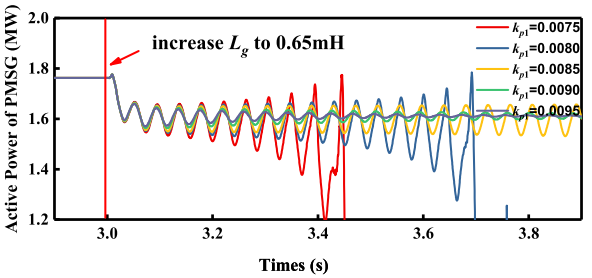


**FIGURE 14.** Active power of the D-PMSG grid-connected system as $k_{p1}$ changes.

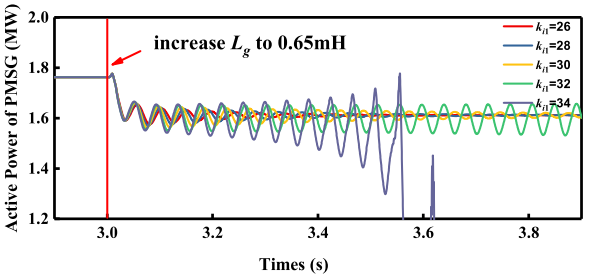


**FIGURE 15.** Active power of the D-PMSG grid-connected system as $k_{i1}$ changes.

### D. THE IMPACT OF THE INTEGRAL GAIN OF THE PLL

The integral gain of the PLL, $k_{i1}$, is set to 26, 28, 30, 32, and 34 to verify the root locus in Section 3.2.3, and the oscillation waveforms of the active power of the system as $k_{i1}$ changes are shown in Fig. 15. Fig. 15 shows that an increase in the integral gain $k_{i1}$ results in a decrease in the damping of the SSO corresponding mode, and the oscillation tends to be divergent. The simulation results agree with the root locus analysis in Section 3.2.3.

## V. CONCLUSION

In this paper, the mechanism of the SSO phenomenon in the D-PMSG grid-connected system is studied. Based on the small signal model, the MIMO transfer functions with $d$- and $q$-axis current references as the inputs and $d$- and $q$-axis components of grid current as the outputs are derived. The root locus analysis of the transfer functions under different parameters and operating conditions of the D-PMSGs is carried out. Then, the root locus analysis of the transfer functions is verified by time-domain simulation. Some conclusions of this paper are as follows. (1) The MIMO transfer functions explain the reason for the SSOs of the D-PMSG grid-connected system. The dynamic process of the PLL and the connection inductance of the grid make the control system of grid-connected inverters have positive feedback, which amplifies the oscillation in the subsynchronous frequency band. (2) The control parameters of grid-connected inverters, the electrical distance of the D-PMSG, and the operation conditions affect the SSO of the system. The risk of SSOs can be reduced by setting reasonable system parameters and load. This paper lays the foundation of studying the mechanism of the SSOs of a D-PMSG system, and offers guidance on the mitigation of SSOs. And theoretically, this

analytical model is also suitable for other grid-connected converters with the same control system, e.g. VSC-HVDC, and the PV system.

## REFERENCES


[1] L. Fan, R. Kavasseri, Z. L. Miao, and C. Zhu, "Modeling of DFIG-based wind farms for SSR analysis," *IEEE Trans. Power Del.*, vol. 25, no. 4, pp. 2073–2082, Oct. 2010.

[2] A. Ostadi, A. Yazdani, and R. K. Varma, "Modeling and stability analysis of a DFIG-based wind-power generator interfaced with a series-compensated line," *IEEE Trans. Power Del.*, vol. 24, no. 3, pp. 1504–1514, Jul. 2009.

[3] L. Fan, C. Zhu, Z. Miao, and M. Hu, "Modal analysis of a DFIG-based wind farm interfaced with a series compensated network," *IEEE Trans. Energy Convers.*, vol. 26, no. 4, pp. 1010–1020, Dec. 2011.

[4] M. Wu, L. Xie, L. Cheng, and R. Sun, "A study on the impact of wind farm spatial distribution on power system sub-synchronous oscillations," *IEEE Trans. Power Syst.*, vol. 31, no. 3, pp. 2154–2162, May 2016.

[5] A. E. Leon, "Integration of DFIG-based wind farms into series-compensated transmission systems," *IEEE Trans. Sustain. Energy*, vol. 7, no. 2, pp. 451–460, Apr. 2016.

[6] B. Huang, H. Sun, Y. Liu, L. Wang, and Y. Chen, "Study on subsynchronous oscillation in D-PMSGs-based wind farm integrated to power system," *IET Renew. Power Gener.*, vol. 13, no. 1, pp. 16–26, Jan. 2019.

[7] H. Liu, X. Xie, J. He, T. Xu, Z. Yu, C. Wang, and C. Zhang, "Subsynchronous interaction between direct-drive PMSG based wind farms and weak AC networks," *IEEE Trans. Power Syst.*, vol. 32, no. 6, pp. 4708–4720, Nov. 2017.

[8] W. Liu, X. Xie, H. Liu, and J. He, "Mechanism and characteristic analyses of subsynchronous oscillations caused by the interactions between direct-drive wind turbines and weak AC power systems," *J. Eng.*, vol. 2017, no. 13, pp. 1651–1656, Jan. 2017.

[9] H. Liu, X. Xie, X. Gao, H. Liu, and Y. Li, "Stability analysis of SSR in multiple wind farms connected to series-compensated systems using impedance network model," *IEEE Trans. Power Syst.*, vol. 33, no. 3, pp. 3118–3128, May 2018.

[10] L. Fan and Z. Miao, "Nyquist-stability-criterion-based SSR explanation for type-3 wind generators," *IEEE Trans. Energy Convers.*, vol. 27, no. 3, pp. 807–809, Sep. 2012.

[11] Z. Yao, P. G. Therond, and B. Davat, "Stability analysis of power systems by the generalised Nyquist criterion," in *Proc. Int. Conf. Control*, Mar. 1994, pp. 739–744.

[12] Z. Miao, "Impedance-model-based SSR analysis for type 3 wind generator and series-compensated network," *IEEE Trans. Energy Convers.*, vol. 27, no. 4, pp. 984–991, Dec. 2012.

[13] B. Wen, D. Boroyevich, R. Burgos, P. Mattavelli, and Z. Shen, "Analysis of D-Q small-signal impedance of grid-tied inverters," *IEEE Trans. Power Electron.*, vol. 31, no. 1, pp. 675–687, Jan. 2016.

[14] B. Wen, D. Boroyevich, P. Mattavelli, Z. Shen, and R. Burgos, "Influence of phase-locked loop on input admittance of three-phase voltage-source converters," in *Proc. 28th Annu. IEEE Appl. Power Electron. Conf. Expo. (APEC)*, Mar. 2013, pp. 897–904.

[15] X. Wang, L. Harnefors, and F. Blaabjerg, "Unified impedance model of grid-connected voltage-source converters," *IEEE Trans. Power Electron.*, vol. 33, no. 2, pp. 1775–1787, Feb. 2018.

[16] T. Bi, J. Li, P. Zhang, E. Mitchell-Colgan, and S. Xiao, "Study on response characteristics of grid-side converter controller of PMSG to subsynchronous frequency component," *IET Renew. Power Gener.*, vol. 11, no. 7, pp. 966–972, Jun. 2017.

[17] Y. Xu and Y. Cao, "Sub-synchronous oscillation in PMSGs based wind farms caused by amplification effect of GSC controller and PLL to harmonics," *IET Renew. Power Gener.*, vol. 12, no. 7, pp. 844–850, May 2018.

[18] H. Wang, Y. Li, and W. Li, "Mechanism research of subsynchronous and supersynchronous oscillations caused by compound current loop of grid-connected inverter," *Power Syst. Technol.*, vol. 41, no. 4, pp. 1061–1067, 2017.

[19] W. Ren and E. Larsen, "A refined frequency scan approach to sub-synchronous control interaction (SSCI) study of wind farms," *IEEE Trans. Power Syst.*, vol. 31, no. 5, pp. 3904–3912, Sep. 2016.

[20] J. Li, T. Bi, and P. Zhang, "Analysis of response characteristics of PMSG-GSC controller to subsynchronous frequency component based on TITO closed loop transfer function," *Power Syst. Technol.*, vol. 42, pp. 3910–3919, Dec. 2018.

[21] H. Zhang, X. Wang, L. Harnefors, H. Gong, J.-P. Hasler, and H.-P. Nee, "SISO transfer functions for stability analysis of grid-connected voltage-source converters," *IEEE Trans. Ind. Appl.*, vol. 55, no. 3, pp. 2931–2941, May 2019.

[22] H. Zhang, L. Harnefors, X. Wang, H. Gong, and J.-P. Hasler, "Stability analysis of grid-connected voltage-source converters using SISO modeling," *IEEE Trans. Power Electron.*, vol. 34, no. 8, pp. 8104–8117, Aug. 2019.

[23] B. Liu, *Modern Control Theory*, 3rd ed. Beijing, China: China Machine Press, 2017, pp. 157–186.


**XIAOFANG WU** received the B.S. degree in electrical engineering from Chongqing University, Chongqing, China, in 2017. She is currently pursuing the Ph.D. degree with Xi'an Jiaotong University. Her research interests include power system stability and stability analysis of renewable energy grid connection systems.

**ZHENGCHUN DU** (Member, IEEE) was born in Shaanxi, China, in 1963. He received the B.S., M.S., and Ph.D. degrees in electrical engineering from Xi'an Jiaotong University, Xi'an, China, in 1983, 1986, and 1993, respectively. He is currently a Professor of electrical engineering with Xi'an Jiaotong University. His research interests include power system stability and control.

**XIAOTIAN YUAN** (Student Member, IEEE) received the B.S. degree in electrical engineering from Xi'an Jiaotong University, Xi'an, China, in 2017, where he is currently pursuing the Ph.D. degree. His research interest includes power system stability and control.

**GUIHONG WU** is currently pursuing the Ph.D. degree with Xi'an Jiaotong University. His research interests include power system stability and control of HVDC transmission.

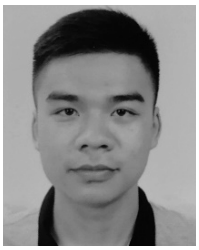

**FENG ZENG** received the B.S. degree in electrical engineering from Xi'an Jiaotong University, Xi'an, China, in 2018, where he is currently pursuing the M.S. degree. His research interests include stability analysis and control of wind power systems.